Research Article Vol. 3, No. 2 / 15 February 2020 / OSA Continuum 275

Dispersive Fourier transform characterization of multipulse dissipative soliton complexes in a mode-locked soliton-similariton laser

CORALINE LAPRE,[1] CYRIL BILLET,[1] FANCHAO MENG,[1] GOËRY GENTY,[2] AND JOHN M. DUDLEY[1,*]

[1] *Institut FEMTO-ST, Université Bourgogne Franche-Comté CNRS UMR 6174, Besançon, 25000, France*
[2] *Photonics Laboratory, Tampere University, Tampere, FI-33104, Finland*
[*] *john.dudley@univ-fcomte.fr*

Abstract: We use the dispersive Fourier transform to spectrally characterize "multipulse soliton complexes" in a dissipative soliton fiber laser operating in the soliton-similariton regime. These multipulse complexes consist of two or more circulating dissipative solitons of picosecond duration, but with temporal separations of ~5–40 ns, three orders of magnitude greater than the individual pulse durations. The results we present include a multipulse complex of 9 distinct single soliton pulses with ~10 ns separation, as well as a multipulse complex where a soliton molecule of two bound pulses separated by ~40 ps coexists with multiple single pulses with separations of ~30 ns. We also use the dispersive Fourier transform to characterize breathing and transition dynamics in this multipulse regime, and our results add further to the experimental characterization of the diverse range of nonlinear structures in dissipative soliton systems.

1. Introduction

Ultrafast mode-locked lasers that exploit nonlinearity in the pulse formation process are well-known to display a rich landscape of "dissipative soliton" dynamics, resulting from the interplay of the nonlinearity with dispersion and dissipation. Although such laser instabilities have been known and studied for many years, their properties have recently received greatly renewed attention because of the development of advanced measurement techniques that allow their single-shot measurement in real-time [1–4]. This has allowed roundtrip-to-roundtrip variations in circulating pulse characteristics to be readily observed, providing a new window into understanding laser instabilities and how they develop.

A technique of this kind that has proven very straightforward to implement experimentally is the dispersive Fourier transform (DFT) that enables measurement of single-shot spectra at MHz repetition rates. The first experiments using DFT to study mode-locked laser instabilities characterized incoherent noise-like fluctuations in a soliton mode-locked fiber laser [5], and this was followed by the measurement of rogue wave fluctuations [6], soliton "explosion" (or collapse and recovery) dynamics [7], and both soliton explosions and chaotic soliton evolution [8].The DFT technique was also applied to a Kerr-lens mode-locked Ti:Sapphire laser, directly allowing pulse build-up from noise to be characterized [3]. Subsequent experiments with a Kerr-lens mode-locked Ti:Sapphire laser reported DFT measurements of spectral interference between closely-spaced pulses in the cavity [9], revealing bound state soliton "molecule" states, known to be characteristic of dissipative soliton laser systems [10–12].

Following these initial experiments, more recent work has applied DFT to wider classes of laser instabilities [4,13–18], further studies on pulse buildup [19–23], characterization of soliton breathing processes [24–28], and the study of bound state soliton molecules [9,29–31]. Another class of dynamics attracting attention in the context of DFT characterization is that of "multipulse soliton complexes." In this regime, the laser operation is associated with two or more

#384501 https://doi.org/10.1364/OSAC.384501
Journal © 2020 Received 26 Nov 2019; revised 12 Jan 2020; accepted 14 Jan 2020; published 28 Jan 2020

OSA CONTINUUM

circulating soliton structures of picosecond duration, but with nanosecond temporal separations [32]. DFT studies of this regime have focussed on a range of different characteristics, including stable double-pulse mode-locking [33], harmonic mode-locking [34], as well as a wide-range of unstable evolution dynamics [35–38].

In this paper, we extend the use of DFT to study such multipulse complexes by reporting their experimental characterization in a soliton-similariton laser where these dynamics have not previously been reported. Our experiments show both the formation of complex states of multiple bound singlet and molecule pulses, as well as breathing multipulse dynamics over 100's of round trips. These results add further to the experimental characterization of the diverse range of nonlinear structures in dissipative soliton systems.

2. Experimental setup and the multipulse regime

Figure 1 shows the experimental setup and illustrates the general properties of the multipulse complexes that we study here. The laser in Fig. 1(a) is a soliton-similariton ring cavity design operating at wavelength ~1555 nm which consists of four key elements: (i) a normal dispersion amplifying erbium doped fiber (EDF) in which self-similar pulse evolution occurs; (ii) standard single-mode fibre (SMF 28) in which soliton evolution occurs; (iii) a saturable absorber based on nonlinear polarization rotation [39] to initiate and sustain mode-locking; (iv) a spectral filter to match soliton and self-similar propagation [40].

In more detail (referring to Fig. 1(a)), the 976 nm pumped EDF has length $L_{AB} = 11$ m and was based on OFS R37003 fibre with group velocity dispersion (GVD) $\beta_2 = +40 \times 10^{-3}$ ps^2 m^{-1}. The lengths of SMF 28 segments with $\beta_2 = -21.7 \times 10^{-3}$ ps^2 m^{-1} are: $L_{BC} = 1$ m, $L_{EF} = 0.42$ m, and $L_{GH} = 6.8$ m. The lengths of HI1060 segments with $\beta_2 = -11.1 \times 10^{-3}$ ps^2 m^{-1} are: $L_{CD} = 0.5$ m and $L_{DE} = 0.5$ m. The length of an HI1060 FLEX segment with $\beta_2 = -7.0 \times 10^{-3}$ ps^2 m^{-1} is $L_{HA} = 1$ m. The net roundtrip cavity dispersion is +0.24 ps^2. The laser repetition rate is 9.5 MHz (cavity round-trip time of 105 ns). The use of the HI1060 fiber-pigtailed output coupler (between points C and E) was in order to have reduced GVD in the output coupling fibre to minimize self-compression of the chirped similariton pulses. However, the use of such HI1060 fiber is not essential, and the laser operates with very similar characteristics using a standard SMF28-based coupler. We also note that when using nonlinear polarization rotation as a saturable absorber mechanism, the overall effective laser output coupling (via the polarizing beam splitter) varies as a function of the polarization adjustment, and this can have an additional influence on the observed dynamics.

The laser output was characterized using a 0.07 nm resolution optical spectrum analyser (OSA, Anristu MS9710B), average power monitoring, and a DFT setup. The DFT temporally disperses an optical pulse such that the stretched temporal intensity has the same form as the pulse spectrum [2]. The stretched signal was detected using a fast photodiode (Miteq DR-125G-A) and real-time oscilloscope (LeCroy 845 Zi-A, 30-GHz channel, 80 GS s^{-1}), with the stretched pulse timebase t related to optical frequency ν by the transformation $2\pi\nu = t/(\beta_2 z)$, with $\beta_2 z$ the total accumulated dispersion in the stretching fiber. Note that we used different stretching fibers in different experiments, and we give the corresponding values below as appropriate. The corresponding spectral resolution (in nm) is conveniently expressed as $\Delta\lambda = (B|D|z)^{-1}$ where $B = 12.5$ GHz is the overall detection bandwidth, and the dispersion parameter $D = -(2\pi c/\lambda^2)\beta_2$ [2]. Of course, when performing DFT measurements it is essential that the propagation in the DCF is strictly linear [2], and this was achieved in our experiments via inline attenuation prior to injection in the DCF. The fidelity of the DFT measurements was confirmed by comparing the averaged spectrum measured on the OSA with the DFT spectrum as discussed below. We also note that some recent studies of fiber laser instabilities have combined DFT characterization with simultaneous ultrafast photodiode characterization of the corresponding temporal pulse trains [27,42]. Combined spectral and spatio-temporal analysis provides additional insight into

OSA CONTINUUM

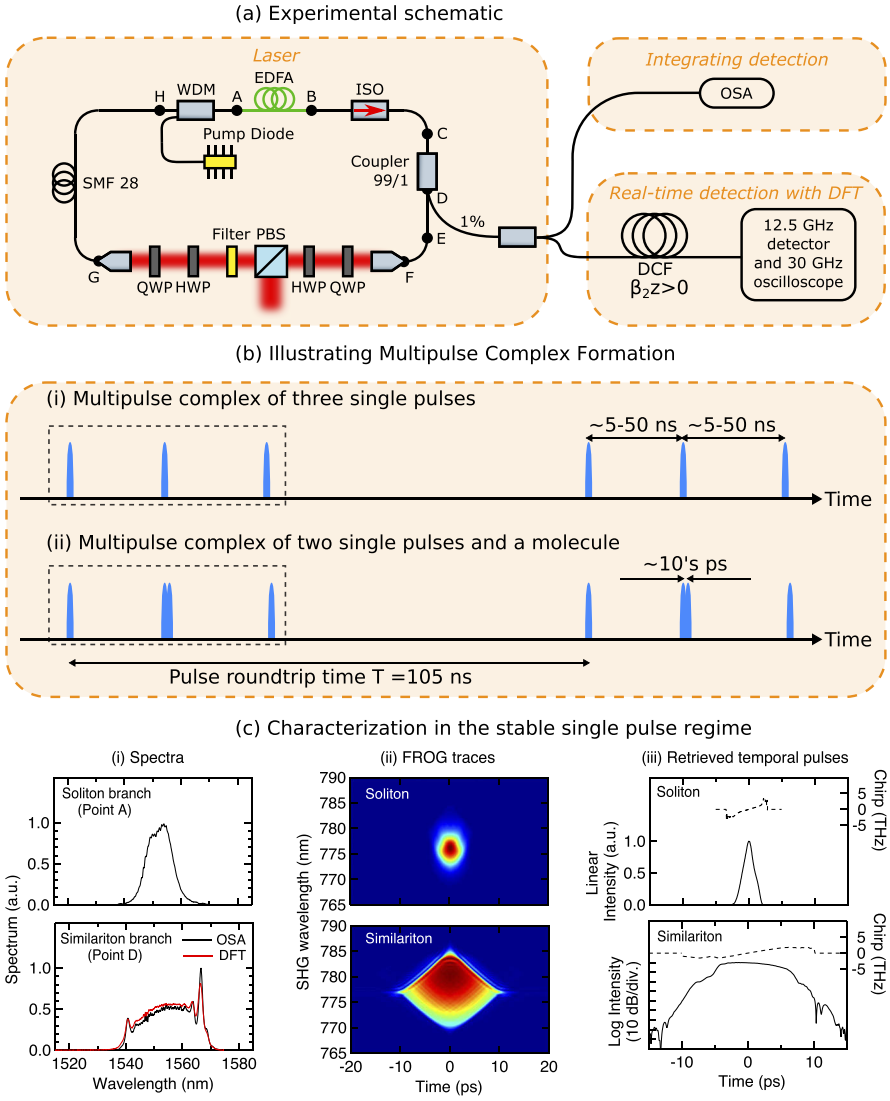

Fig. 1. (a) Setup: EDF, Erbium-doped fibre; ISO, optical isolator; WDM, wavelength-division multiplexer, QWP, quarter-wave plate; HWP, half-wave plate; PBS, polarizing beamsplitter; OSA, optical spectrum analyzer; FROG, frequency-resolved optical gating; DCF, dispersion-compensating fibre; DFT, dispersive Fourier transform. The intracavity filter had 10 nm bandwidth. Further details of the setup are in Ref. [41]. (b) Illustrating the temporal structure of the observed multipulse complexes. (i) The dashed box shows a complex of three distinct (picosecond) pulses separated by 5–40 ns; (ii) Shows a similar complex but where one of the constituent components is a soliton molecule consisting of two pulses separated by ∼10's of ps. (c) Pulse characterization in the stable regime for: (top) the soliton branch (at point A); (bottom) the similariton branch after the EDFA (at point D) showing: (i) Spectra, (ii) FROG traces, (iii) retrieved intensity (solid line, left axis) and chirp (dashed line, right axis). For the similariton spectra we compare OSA (black) and DFT (red) measurements, and we use a logarithmic scale for the similariton intensity to emphasis the low-amplitude wings.

OSA CONTINUUM

the dynamics, but our experiments here are focussed on DFT measurements [9,15,43]. These readily allow us to extract both the number of multiple pulses, their nanosecond scale temporal separation, and their spectral content and evolution.

Previous studies of this laser in Ref. [41] focussed on characterizing operating regimes with only one circulating pulse or one molecule in the cavity. These regimes corresponded to pump powers in the range 30–80 mW, associated with linearly-chirped similariton pulses at the EDF output of duration ~7–10 ps and spectral bandwidths ~20–25 nm. Higher pump powers and/or detuned waveplate positions in the saturable absorber led to more unstable dynamics, but still with only one intracavity circulating pulse.

The results we report here were obtained by studying the laser operation over a wider parameter range of pump power and waveplate positions, which yielded the observation of multipulse complexes as illustrated schematically in Fig. 1(b). For example, Fig. 1(b-i) illustrates a complex of 3 distinct solitons, where the individual pulses have characteristics comparable to those seen in the single-pulse regime (i.e. bandwidths ~20–25 nm and picosecond duration), but with temporal separations ~25–40 ns, orders of magnitude larger than the pulse duration, but still less than the cavity roundtrip time. Experimentally, the exact temporal separations observed varied with both pump power and the orientation of the waveplates, even when varied over only a few degrees. In addition to multipulse complexes consisting only of single picosecond pulses, we also recorded cases where both single soliton pulses and soliton molecules co-existed, as illustrated in Fig. 1(b-ii). Here, the distinct pulses have picosecond duration, the separation in the bound state molecule is also picosecond duration, but again the separation between these different picosecond components of the complex is ~5–40 ns.

Although Fig. 1(b) is only a schematic illustration, experimental results for similar cases are presented below. In this regard, we remark that the DFT is ideally suited to characterize the sequential spectra of pulses that form a multipulse complex, as the DFT measurement yields both the spectra of each pulse in the state, as well as their temporal separation. It is of course necessary in this case that the amount of dispersive stretching for each pulse in the complex is less than the separation between successive pulses so that there is no spectral overlap. Yet at the same time, it is desirable to optimise the amount of stretching that occurs to improve spectral resolution. As we shall see below, we implemented the DFT using different stretching fibres with different values of $\beta_2 z$ depending on the particular characteristics of the multipulse complexes observed under different conditions.

Finally in discussing the experimental setup, for completeness we show in Fig. 1(c) results of second harmonic generation (SHG) frequency-resolved optical gating (FROG) measurements [44,45] in the stable single-pulse laser regime. These illustrate pulse characteristics for: (top) the soliton branch (at point A) and (bottom) the similariton branch after the EDFA (at point D). In each case we show: (i) spectra, (ii) FROG traces, (iii) retrieved intensity (solid line, left axis) and chirp (dashed line, right axis). For the similariton spectra we compare OSA (black) and DFT (red) measurements as this comparison provides a stringent test of the fidelity of the DFT technique. Note that the similariton results were previously also described in Ref. [41].

The spectral and temporal characteristics of the pulses in the two branches of the cavity are clearly very different, with the contrast in the localization characteristics especially apparent in the FROG traces. We also note that the spectrum of the pulse from the similariton branch in Fig. 1(c-i) shows pronounced spectral modulation peaks particularly on the long wavelength edge. Such spectral features are typical of similariton pulses (and indeed pulses from many other normal dispersion fibre laser designs) as previously noted by several authors [26,46]. The physical origin of these peaks is both due to the intrinsic nature of the chirp across the pulse that induces spectral modulation because of the interference of two waves of the same frequency but different phases [47], as well as the effect of spectral filtering [46]. For our laser, the long wavelength peak appears enhanced because of asymmetric amplifier gain. In particular, the gain maxima

OSA CONTINUUM

in an EDF depends on factors such as the active ion dopant level, the pump power and pump geometry, as well as the fiber length, and can be shifted to either longer or shorter wavelengths depending on the particular configuration used [48]. In our case, the gain maxima was observed around 1570 nm which leads to the enhancement of the long wavelength modulation peak.

Concerning the retrieved temporal characteristics in Fig. 1(c-iii), the similariton pulse (FWHM ~8.2 ps) shows the expected strong linear chirp and rapid fall-off in the temporal intensity, and we use a logarithmic intensity scale to emphasize the decaying wings of the pulse (characteristic of self-similar evolution [49]). As expected, the soliton is significantly shorter (FWHM ~2.1 ps) and we also see that it shows a linear chirp. This is due to the particular design of our cavity where we operate not with a fundamental soliton but with a soliton order N ~2 such that we see significant evolution in the anomalous dispersion soliton branch. Further details and numerical simulations of the intracavity pulse evolution in the cavity are given in Ref. [41]. We also note here that FROG measurements are not possible for the multipulse complexes studied here because the measured trace will be integrated over multiple pulses that will not necessarily possess identical characteristics. Nonetheless, intensity autocorrelation measurements were carried out to obtain an indication of a characteristic timescale associated with the multipulse states, and the spectral bandwidths ~20–25 nm reported below corresponding to measured intensity autocorrelation widths in the range 8–10 ps.

3. Results

Our first DFT results are shown in Fig. 2. These measurements were made with dispersion $\beta_2 z = +468\,\mathrm{ps}^2$ and corresponding spectral resolution of 0.22 nm. For Fig. 2(a), the results were obtained with a 976 nm pump power of 82 mW (just above the stable single-pulse regime) and an output power of 0.3 mW. The results show the DFT characterization of a complex state consisting of two distinct solitons separated by ~42 ns where we show (bottom) a false-color plot of successive DFT measurements over 200 roundtrips, and (top) one typical spectral profile (taken from the first roundtrip of the sequence). The two temporally-separated spectra here exhibit near-identical characteristics with spectral width of 23 nm and a spectral structure consistent with linearly-chirped parabolic pulse dissipative solitons [41]. The bottom axes of the false-color plot and the extracted spectral profiles directly show the DFT timebase in nanoseconds (to illustrate the temporal separation), but we also include a wavelength scale for the extracted spectral profiles using the appropriate time-to-wavelength mapping. Because of the large number and close spacing of the pulses seen in some of our multipulse states it is not practical to provide a separate wavelength scale for each constituent spectrum, but the wavelength scale shown in the upper plots also applies to the false-color DFT data. The central wavelength (determined from averaged OSA measurements) was 1555 nm. Note that the direction of increasing wavelength and time in these figures is reversed because of the sign of dispersion in the DFT stretching fiber.

Figure 2(b) plots similar data at a significantly higher pump power of 270 mW and a higher output power of 1 mW. These results show a remarkable complex of 9 pulses simultaneously circulating in the cavity, all with comparable spectral widths of ~18.5 nm but with non-identical temporal separations ranging from 9.7–12.0 ns. To our knowledge, such a multipulse complex with 9 pulses has not previously been characterized using DFT. Although we plot the DFT results in Fig. 2(a) and (b) over only 200 roundtrips, the multipulse states were stable over the full data acquisition of 4000 roundtrips and indeed, were observed to be essentially indefinitely stable over much longer timescales (operating periods of ~hours) until the laser cavity parameters were modified. Similar degrees of long-term stability were also observed for the results below in Figs. 3 and 4.

Figure 3 presents results for a different class of multipulse complex where one of the constituent structures is a dissipative soliton molecule. We again show (bottom) a false-color plot of successive DFT measurements over 200 roundtrips, and (top) one typical spectral profile from the first

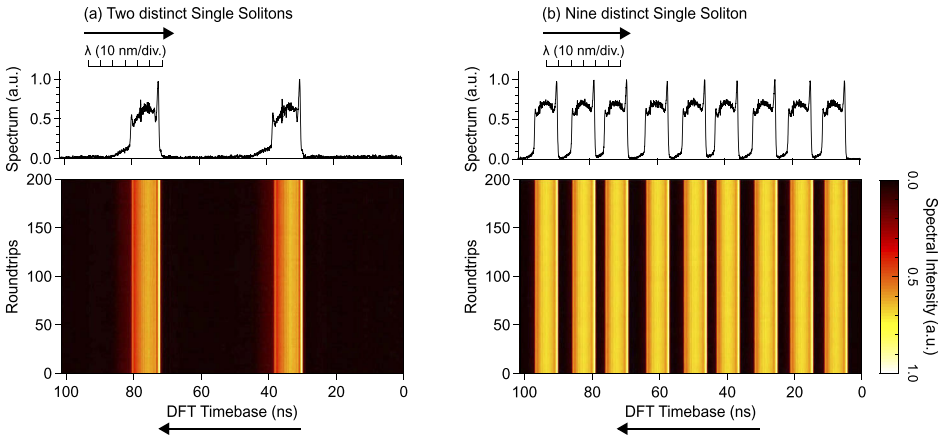

Fig. 2. Multipulse complex consisting of distinct single pulses showing (a) 2 single pulses and (b) 9 single pulses circulating in the cavity. The bottom subfigure in each case superposes results from DFT measurements over 200 cavity rountrips while the top figure shows the spectral profile taken from the first roundtrip of the data sequence. The DFT timebase is plotted over the 105 ns range of a cavity roundtrip, while we also show the calibrated wavelength axis in nm when plotting the extracted spectra. The central wavelength is 1555 nm.

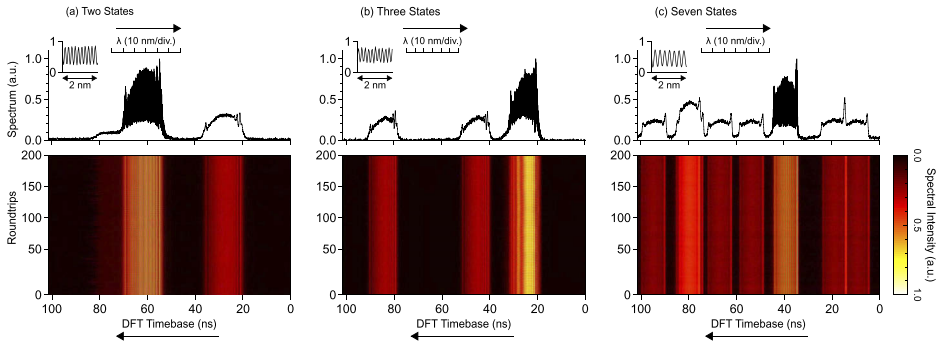

Fig. 3. Multipulse complexes that include a soliton molecule. (a) a molecule state and a distinct single pulse, (b) a molecule state and 2 distinct single pulses, (c) a molecule state and 7 distinct single pulses. The larger amplitude of the pulse around 80 ns is attributed to the incoherent superposition of two solitons. The insets in all cases show the fringes of the molecule structure over a 2 nm span near the spectral centre of 1555 nm.

roundtrip of the sequence. For example, considering the results in Fig. 3(a), we again see how the recorded DFT trace again consists of a series of two distinct structures separated by ~10's of nanoseconds, but whilst the spectrum centred on ~25 ns is qualitatively similar to the results shown in Fig. 2, the spectrum centred on ~60 ns exhibits a clear spectral modulation signature of a molecule state [9]. These measurements used a DFT dispersion $\beta_2 z = +610\,\mathrm{ps}^2$ and spectral resolution of 0.17 nm. The inset highlights the fringes of the molecule structure over a 2 nm span near the spectral centre, with the 0.19 nm fringe spacing corresponding to a ~42 ps separation between the constituent molecule components. The fringe contrast of 70% in these measurements is attributed to the finite resolution of the DFT [41]. These results were obtained with a pump power of 175 mW, a laser output power of 0.6 mW, and the bandwidth of the individual pulses increased from that seen above in Fig. 2 to ~33 nm.

OSA CONTINUUM

The results in Fig. 3(b) were obtained at a pump power of 270 mW and corresponding higher output power of 1 mW. These are in fact identical power values as those for the results in Fig. 2(b) but the qualitative behaviour of the laser here is significantly different because the laser was operated with different waveplate orientations. In particular, the results now show two single pulses coexisting with a molecule state. Note that we use a reduced DFT dispersion $\beta_{2z} = +468\,\mathrm{ps}^2$ to avoid temporal overlap between the spectra. This of course leads to reduced spectral resolution of 0.22 nm compared to Fig. 3(a), and we see this in the slightly lower fringe contrast of 62%. The fringe spacing here is again 0.19 nm corresponding to a pulse separation of ~42 ps between the molecule components. The individual spectral width of the pulses here is ~32 nm, comparable to that seen in Fig. 3(a).

For another orientation of the waveplates at the same power level (in particular by adjusting the quarter-wave plate positioned after the spectral filter) additional pulses were seen to coexist in the cavity as shown in Fig. 3(c). In this case, we plot results for a higher DFT dispersion of $\beta_{2z} = +610\,\mathrm{ps}^2$ [as in Fig. 3(a)] to illustrate the issue of temporal overlap that can occur when measuring multiple pulses. In discussing these results, we first remark that we clearly see the presence of a molecule structure, and the fringe spacing here is 0.27 nm corresponding to a pulse separation of ~30 ps between the molecule components. We then see a sequence of additional distinct single pulses with non-identical separations in the range 9.5–21.2 ns, and we note the temporal overlap between the measured spectra around a DFT timebase value of ~10 ns. The structure centred on the DFT timebase value of ~80 ns has around twice the intensity of the neighbouring spectra, but in fact a detailed examination of the spectral peaks in this case reveal that this structure in fact corresponds to two pulses, with a very small separation of 1.3 ns.

In addition to the stable states described above, it was also possible to capture regimes where the multipulse complexes would "breathe" over 50–100 roundtrips, and Fig. 4 shows typical results. In this case, the figure again shows a false-color sequence of DFT spectra (over 400 roundtrips), and we also show extracted spectral profiles at two selected roundtrips at points of minimum and maximum spectral expansion (see caption for details). The results in Fig. 4(a) were obtained for 175 mW pump power and 0.6 mW output power (the same power levels as in Fig. 3(a)) but with a particular waveplate orientation where breathing was observed. The DFT dispersion was $\beta_{2z} = +257\,\mathrm{ps}^2$ (spectral resolution of 0.40 nm). Figure 4(a) shows a breathing state of 3 pulses, and for the same waveplate positions but a higher pump power of 285 mW (1 mW output power), Fig. 4(b) shows similar behaviour, but with 4 pulses per roundtrip.

These measurements of spectral breathing in the multipulse regime are complementary to those reported in other recent studies [26,27]. We note in this context that the results reported in Ref. [27] were noteworthy in including experimental measurements of corresponding periodic evolution in the time-domain, and also in using numerical simulations based on the complex cubic quintic Ginzberg-Landau equation to relate the physical origin of the breathing to the presence of the higher-order (quintic) gain term in the nonlinear model. Gain saturation was also found to play a role in another numerical study of similar behaviour [50].

Finally, in addition to results above showing stable or breathing multipulse complexes, we have also used DFT measurements to characterize a novel regime of transition instability dynamics around the position of stable multipulse operation. These results were recorded at a pump power of 175 mW as in Fig. 3(a) where we previously observed a stable single pulse-molecule complex. However, with waveplate detuning from this stable point, the laser entered into a regime of large amplitude spectral fluctuations. The DFT characterisation that captured this behavior is shown in Fig. 5 where we plot: (a) a sequence of DFT measurements over 3900 roundtrips that shows a series of unstable but localized pulses in the cavity up to ~1700 roundtrips, followed by collapse and the appearance of a chaotic spectrum. We were able to characterize only 3900 roundtrips in this regime because of oscilloscope storage limitations, and within this constraint (even with further parameter adjustment) we were unable to observe any evidence that the multipulse to

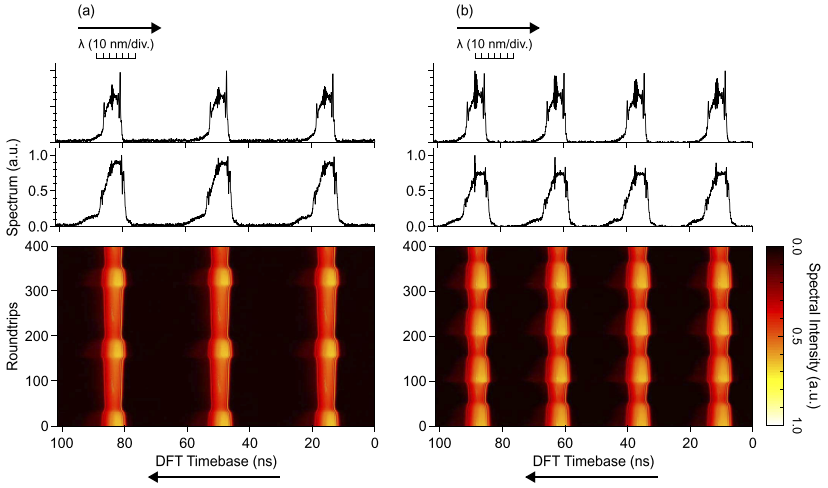

Fig. 4. Multipulse complexes exhibiting breathing dynamics. (a) Three single pulses (b) Four single pulses. The bottom figures show a sequence of measured DFT spectra over 400 roundtrips. The top figures show spectra at two selected roundtrips at points of minimum and maximum spectral expansion: (a) Roundtrips 158 and 203 respectively; (b) Roundtrips 102 and 163 respectively.

chaos transition was reversible or periodic. However, the study of potential intermittence in this regime may well be observable over longer timescales, as it is readily see in other classes of dynamics with this laser system [41].

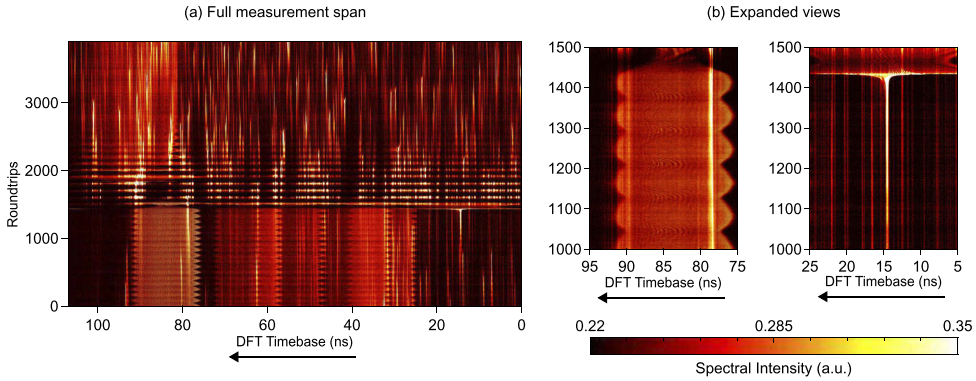

Fig. 5. Experimental DFT characterization of unstable dynamics in the multipulse regime. (a) shows measurements over 3900 roundtrips and the full 105 ns DFT timebase, illustrating unstable but localized multiple pulses up to ~1700 roundtrips followed by chaotic evolution. The expanded views in (b) show a short-lived quasi-stable breathing molecule structure (left, around a DFT timebase value of ~85 ns) and the clear spectral expansion signature of a soliton explosion (right, around DFT timebase of ~15 ns).

Several other features of the initial evolution regime are noteworthy. We show the evolution over roundtrips 1000-1500 for a DFT timebase value of ~85 ns in the expanded view in the left panel of Fig. 5(b), where we see a molecule structure that is well localized but which "breathes" with roundtrips. Related behaviour was reported in Refs [27,38] and linked to energy exchange between the molecule components associated with gain dynamics effects. For a DFT timebase

OSA CONTINUUM

value of ~15 ns, the results in the right panel of Fig. 5(b) show rapid spectral expansion, and we note that this is very similar to the dynamics usually associated with below-threshold build up from noise, where the pulse energy dramatically changes before balance is reached between gain and loss, and dispersion and nonlinearity [23,33,41,51]. We also note the "on-off" behaviour seen between roundtrips 1500-2000 (across the full measurement window) which can be interpreted in terms of a Q-switching-like instability [23,33], and the multiple discrete lines in the chaotic regime that appear to be a universal feature of unstable dissipative soliton lasers [3,19,20,22,52].

4. Discussion and conclusions

In this paper, we have reported an experimental characterization of a range of "multipulse soliton complexes" in a dissipative soliton fiber laser operating in the soliton-similariton regime. The multipulse complexes included up to 9 picosecond-scale soliton structures simultaneously oscillating in the cavity, with the observed soliton structures also including bound state soliton molecules. This operating regime was observed at pump power levels greater than those associated with stable single pulse operation, and the detailed nature of the multipulse complexes observed depended sensitively on the orientation of the waveplates used to control the properties of the laser saturable absorber segment. Multipulse breather structures were also observed, and the study of an instability regime revealed the presence of breathing soliton molecules and soliton explosions.

These results provide further evidence of the rich dynamics that are present in dissipative soliton mode-locked lasers, and extend the experimental studies of highly complex multiple pulse structures. In particular, although features such as soliton molecule breathing, rapid spectral expansion and Q-switching have been reported separately in other studies of mode-locked lasers [16,23,24,26,27,51], their simultaneous appearance during the transition dynamics between stable and unstable multipulse oscillation is further confirmation of their ubiquitous nature in the dynamical landscape of dissipative soliton systems.

It is important to stress in this context that such experiments are only possible because of the measurement capability provided by DFT spectral characterization, and our results provide yet another example of the importance of real-time measurements to gain improved insights into nonlinear dynamical sytems. Of particular interest in future studies will be the systematic use of simultaneous temporal characterisation to develop an even more complete picture of the dynamics [4,27,42].

Funding

Agence Nationale de la Recherche (ANR-15-IDEX-0003, ANR-17-EURE-0002); Academy of Finland (298463, 318082, Flagship PREIN).

Disclosures

The authors declare no conflicts of interest.

References

1. D. R. Solli, C. Ropers, P. Koonath, and B. Jalali, "Optical rogue waves," Nature **450**(7172), 1054–1057 (2007).
2. K. Goda and B. Jalali, "Dispersive Fourier transformation for fast continuous single-shot measurements," Nat. Photonics **7**(2), 102–112 (2013).
3. G. Herink, B. Jalali, C. Ropers, and D. R. Solli, "Resolving the build-up of femtosecond mode-locking with single-shot spectroscopy at 90 MHz frame rate," Nat. Photonics **10**(5), 321–326 (2016).
4. P. Ryczkowski, M. Närhi, C. Billet, J. M. Merolla, G. Genty, and J. M. Dudley, "Real-time full-field characterization of transient dissipative soliton dynamics in a mode-locked laser," Nat. Photonics **12**(4), 221–227 (2018).
5. A. F. J. Runge, C. Aguergaray, N. G. R. Broderick, and M. Erkintalo, "Coherence and shot-to-shot spectral fluctuations in noise-like ultrafast fiber lasers," Opt. Lett. **38**(21), 4327–4330 (2013).

OSA CONTINUUM

6. A. F. J. Runge, C. Aguergaray, N. G. R. Broderick, and M. Erkintalo, "Raman rogue waves in a partially mode-locked fiber laser," Opt. Lett. **39**(2), 319–322 (2014).
7. A. F. J. Runge, N. G. R. Broderick, and M. Erkintalo, "Observation of soliton explosions in a passively mode-locked fiber laser," Optica **2**(1), 36–39 (2015).
8. M. Liu, A.-P. Luo, Y.-R. Yan, S. Hu, Y.-C. Liu, H. Cui, Z.-C. Luo, and W.-C. Xu, "Successive soliton explosions in an ultrafast fiber laser," Opt. Lett. **41**(6), 1181–1184 (2016).
9. G. Herink, F. Kurtz, B. Jalali, D. R. Solli, and C. Ropers, "Real-time spectral interferometry probes the internal dynamics of femtosecond soliton molecules," Science **356**(6333), 50–54 (2017).
10. B. A. Malomed, "Bound solitons in the nonlinear Schrödinger-Ginzburg-Landau equation," Phys. Rev. A **44**(10), 6954–6957 (1991).
11. N. Akhmediev and A. Ankiewicz, *Solitons: Non-linear pulses and beams (Optical and Quantum Electronics Series, 5)* (Chapman & Hall, 1997).
12. P. Grelu, F. Belhache, F. Gutty, and J.-M. Soto-Crespo, "Phase-locked soliton pairs in a stretched-pulse fiber laser," Opt. Lett. **27**(11), 966–998 (2002).
13. B. Li, Y. Yu, X. Wei, Y. Xu, K. K. Tsia, and K. K. Y. Wong, "Real-time observation of round-trip resolved spectral dynamics in a stabilized fs fiber laser," Opt. Express **25**(8), 8751–8759 (2017).
14. A. Klein, G. Masri, H. Duadi, K. Sulimany, O. Lib, H. Steinberg, S. A. Kolpakov, and M. Fridman, "Ultrafast rogue wave patterns in fiber lasers," Optica **5**(7), 774–778 (2018).
15. M. Suzuki, O. Boyraz, H. Asghari, P. Trinh, H. Kuroda, and B. Jalali, "Spectral periodicity in soliton explosions on a broadband mode-locked Yb fiber laser using time-stretch spectroscopy," Opt. Lett. **43**(8), 1862–1865 (2018).
16. Z.-W. Wei, M. Liu, S.-X. Ming, A.-P. Luo, W.-C. Xu, and Z.-C. Luo, "Pulsating soliton with chaotic behavior in a fiber laser," Opt. Lett. **43**(24), 5965–5968 (2018).
17. S. D. Chowdhury, B. D. Gupta, S. Chatterjee, R. Sen, and M. Pal, "Rogue waves in a linear cavity Yb-fiber laser through spectral filtering induced pulse instability," Opt. Lett. **44**(9), 2161–2164 (2019).
18. J. Peng and H. Zeng, "Soliton collision induced explosions in a mode-locked fibre laser," Commun. Phys. **2**(1), 34 (2019).
19. J. Peng, M. Sorokina, S. Sugavanam, N. Tarasov, D. V. Churkin, S. K. Turitsyn, and H. Zeng, "Real-time observation of dissipative soliton formation in nonlinear polarization rotation mode-locked fibre lasers," Commun. Phys. **1**(1), 20 (2018).
20. X. Liu, X. Yao, and Y. Cui, "Real-Time Observation of the Buildup of Soliton Molecules," Phys. Rev. Lett. **121**(2), 023905 (2018).
21. X. Wang, X. Ren, J. Peng, X. Shen, K. Huang, M. Yan, and H. Zeng, "On the Q-switching bunch dynamics in the build-up of stretched-pulse mode-locking," Opt. Express **27**(3), 2747–2753 (2019).
22. X. Liu and Y. Cui, "Revealing the behavior of soliton buildup in a mode-locked laser," Adv. Photonics **1**(1), 016003 (2019).
23. Y. Cui and X. Liu, "Revelation of the birth and extinction dynamics of solitons in SWNT-mode-locked fiber lasers," Photonics Res. **7**(4), 423–430 (2019).
24. Z. Wang, Z. Wang, Y. Liu, R. He, J. Zhao, G. Wang, and G. Yang, "Self-organized compound pattern and pulsation of dissipative solitons in a passively mode-locked fiber laser," Opt. Lett. **43**(3), 478–481 (2018).
25. Y. Du, Z. Xu, and X. Shu, "Spatio-spectral dynamics of the pulsating dissipative solitons in a normal-dispersion fiber laser," Opt. Lett. **43**(15), 3602–3605 (2018).
26. X. Wang, Y. Liu, Z. Wang, Y. Yue, J. He, B. Mao, R. He, and J. Hu, "Transient behaviors of pure soliton pulsations and soliton explosion in an L-band normal-dispersion mode-locked fiber laser," Opt. Express **27**(13), 17729–17742 (2019).
27. J. Peng, S. Boscolo, Z. Zhao, and H. Zeng, "Breathing dissipative solitons in mode-locked fiber lasers," Sci. Adv. **5**(11), eaax1110 (2019).
28. J. Peng and H. Zeng, "Experimental observations of breathing dissipative soliton explosions," Phys. Rev. Appl. **12**(3), 034052 (2019).
29. K. Krupa, K. Nithyanandan, U. Andral, P. Tchofo-Dinda, and P. Grelu, "Real-Time Observation of Internal Motion within Ultrafast Dissipative Optical Soliton Molecules," Phys. Rev. Lett. **118**(24), 243901 (2017).
30. J. Peng and H. Zeng, "Dynamics of soliton molecules in a normal-dispersion fiber laser," Opt. Lett. **44**(11), 2899–2902 (2019).
31. Z. Wang, K. Nithyanandan, A. Coillet, P. Tchofo-Dinda, and P. Grelu, "Optical soliton molecular complexes in a passively mode-locked fibre laser," Nat. Commun. **10**(1), 830 (2019).
32. L. Li, H. Huang, L. Su, D. Shen, D. Tang, M. Klimczak, and L. Zhao, "Various soliton molecules in fiber systems," Appl. Opt. **58**(10), 2745–2753 (2019).
33. S. Sun, Z. Lin, W. Li, N. Zhu, and M. Li, "Time-stretch probing of ultra-fast soliton dynamics related to Q-switched instabilities in mode-locked fiber laser," Opt. Express **26**(16), 20888–20901 (2018).
34. X. Liu and M. Pang, "Revealing the buildup dynamics of harmonic mode-locking states in ultrafast lasers," Laser Photonics Rev. **13**(9), 1800333 (2019).
35. Y. Yu, B. Li, X. Wei, Y. Xu, K. K. M. Tsia, and K. K. Y. Wong, "Spectral-temporal dynamics of multipulse mode-locking," Appl. Phys. Lett. **110**(20), 201107 (2017).

OSA CONTINUUM

36. Y. Yu, Z. Luo, J. Kang, and K. K. Wong, "Mutually ignited soliton explosions in a fiber laser," Opt. Lett. **43**(17), 4132–4135 (2018).
37. Y. Luo, Y. Xiang, T. Liu, B. Liu, R. Xia, Z. Yan, X. Tang, D. Liu, Q. Sun, and P. P. Shum, "Real-time access to the coexistence of soliton singlets and molecules in an all-fiber laser," Opt. Lett. **44**(17), 4263–4266 (2019).
38. X. Wang, J. He, B. Mao, H. Guo, Z. Wang, Y. Yue, and Y. Liu, "Real-time observation of dissociation dynamics within a pulsating soliton molecule," Opt. Express **27**(20), 28214–28222 (2019).
39. D. Noske, N. Pandit, and J. Taylor, "Subpicosecond soliton pulse formation from self-mode-locked erbium fibre laser using intensity dependent polarisation rotation," Electron. Lett. **28**(23), 2185–2186 (1992).
40. R. I. Woodward, "Dispersion engineering of mode-locked fibre lasers," J. Opt. **20**(3), 033002 (2018).
41. C. Lapre, C. Billet, F. Meng, P. Ryczkowski, T. Sylvestre, C. Finot, G. Genty, and J. M. Dudley, "Real-time characterization of spectral instabilities in a mode-locked fibre laser exhibiting soliton-similariton dynamics," Sci. Rep. **9**(1), 13950 (2019).
42. H.-J. Chen, Y.-J. Tan, J.-G. Long, W.-C. Chen, W.-Y. Hong, H. Cui, A.-P. Luo, Z.-C. Luo, and W.-C. Xu, "Dynamical diversity of pulsating solitons in a fiber laser," Opt. Express **27**(20), 28507–28522 (2019).
43. J. Zeng and M. Y. Sander, "Real-time transition dynamics between multi-pulsing states in a mode-locked fiber laser," Opt. Lett. **45**(1), 5–8 (2020).
44. R. Trebino, *Frequency-Resolved Optical Gating: The Measurement of Ultrashort Laser Pulses* (Springer, 2002).
45. J. M. Dudley, L. P. Barry, J. D. Harvey, M. D. Thomson, B. C. Thomsen, P. G. Bollond, and R. Leonhardt, "Complete characterization of ultrashort pulse sources at 1550 nm," IEEE J. Quantum Electron. **35**(4), 441–450 (1999).
46. A. Chong, W. H. Renninger, and F. W. Wise, "Properties of normal-dispersion femtosecond fiber lasers," J. Opt. Soc. Am. B **25**(2), 140–148 (2008).
47. G. P. Agrawal, *Nonlinear Fiber Optics* (Academic Press, 2013).
48. E. Desurvire, *Erbium-doped fiber amplifiers: principles and applications* (Wiley, 1994).
49. J. M. Dudley, C. Finot, D. J. Richardson, and G. Millot, "Self-similarity in ultrafast nonlinear optics," Nat. Phys. **3**(9), 597–603 (2007).
50. R. He, Z. Wang, Y. Liu, Z. Wang, H. Liang, S. Han, and J. He, "Dynamic evolution of pulsating solitons in a dissipative system with the gain saturation effect," Opt. Express **26**(25), 33116–33128 (2018).
51. H.-J. Chen, M. Liu, J. Yao, S. Hu, J.-B. He, A.-P. Luo, W.-C. Xu, and Z.-C. Luo, "Buildup dynamics of dissipative soliton in an ultrafast fiber laser with net-normal dispersion," Opt. Express **26**(3), 2972–2982 (2018).
52. J. Peng, L. Zhan, Z. Gu, J. Liu, S. Luo, X. Shen, and Q. Shen, "Modulation Instability in Dissipative Soliton Fiber Lasers and Its Application on Cavity Net Dispersion Measurement," J. Lightwave Technol. **30**(16), 2707–2712 (2012).